EasyTopo: A toolbox for rapid diffuse optical topography based on a standard template of brain atlas

Fenghua Tian*, Zi-Jing Lin, Hanli Liu
Department of Bioengineering, University of Texas at Arlington, 500 UTA Blvd, Arlington, TX, USA 76019

ABSTRACT

Diffuse optical topography remains a valid tool in functional near infrared spectroscopy (fNIRS) since it avoids solving the forward and inverse computational problems, which are encountered in diffuse optical tomography. Topography is particularly useful when a sparse array of optodes is used and depth specificity is not the primary interest. We have developed an easy toolbox for diffuse optical topography ("EasyTopo") based on a standard template of brain atlas. EasyTopo approximates the cortical layer of the brain as a hemispherical surface. Therefore, the stereotaxic coordinates of the brain surface and the co-registered fNIRS measurements (channels) are converted into the spherical coordinates, where 2D angular interpolation of the channel-wise data is implemented to obtain a topographic image of brain activation in the latitude-longitude space. Then, the interpolated image is projected back onto the brain surface in the original 3D stereotaxic coordinates. Compared with the existing 3D topography methods, EasyTopo is more computationally efficient and does not require any data extrapolation. Another advantage of EasyTopo is that the data between two spatially adjacent channels are interpolated along their included angles (i.e., along the angular direction) rather than along a straight line going under the brain surface. The former geometry in principle matches better with the realistic brain structure than the latter one. EasyTopo has been validated with both simulation and human experiments. Now this toolbox is publically available.

Keywords: Functional near infrared spectroscopy (fNIRS), topography, EasyTopo, angular interpolation

1. INTRODUCTION

Functional near infrared spectroscopy (fNIRS) is an emerging neuroimaging technology that uses low-power near infrared light (650 to 950 nm) to measure the changes of cerebral blood flow and oxygenation. The near infrared light is mainly absorbed by oxygenated hemoglobin (HbO_2) and deoxygenated hemoglobin (Hb) in the blood. The near infrared spectroscopy (NIRS) methods to measure hemodynamic changes in the brain associated with neuronal activation were first described in 1993 [1,2,3]. Early studies used a sparse array of optodes (i.e., light sources and detectors) to distinguish brain activation in different regions. Diffuse optical topography of the brain activation was attained by interpolating the hemodynamic signals between adjacent measurement channels [4,5]. Its spatial resolution was comparable to the source-detector separation that was in a few centimeters. Recently the technology has been advanced to high-density diffuse optical tomography [6,7] which records data in a broad range of source-detector separations and reconstructs volumetric images of brain activation by solving the forward and inverse problems of light propagation. While high-density diffuse optical tomography improves the spatial resolution and positional accuracy of optical brain imaging [8,9,10], it also increases the weight of the probe and the preparation time to attach the probe on a subject's head.

To date, a sparse optode array is still widely used in clinically oriented studies as a compromise between the image quality and the comfort of subjects as well as the experimental setup time. Given the sparsity of measurements in these applications, diffuse optical topography remains a valid tool because it avoids solving the forward and inverse problems of light propagation that are computationally intensive. In early studies using the topographic approach [4,5], however, data was interpolated in a flat surface which significantly deviated from the realistic human brain anatomy. In order to localize and identify the activated regions in the brain more accurately, recent studies have incorporated topography with a standard template of brain atlas [11,12]. For brain template-based topography, currently the data is interpolated on a stereotaxic convex defined by a cohort of 2D surfaces, which indeed does not match the surface of the brain perfectly. Sometimes the data have to be further extrapolated.

*fenghua.tian@gmail.com

In this study, we have developed and validated a toolbox for rapid diffuse optical topography ("EasyTopo") of brain activation. Based on a hemispherical approximation of the brain, EasyTopo implemented 2D angular interpolation in a spherical coordinate system. Compared with the other brain template-based topography methods [11,12], EasyTopo is more computationally efficient and does not require any data interpolation/extrapolation in 3D stereotaxic space. In addition, the angular interpolation used in EasyTopo is more physiologically meaningful and agrees better with the reality. While EasyTopo has been briefly introduced in our previous report [13], here we will describe the methods and the validation results in details.

2. METHODS

2.1 Brain template and co-registration

We used a standard MRI template of the brain, known as ICBM 152 nonlinear asymmetric template, in a spatial resolution of 1×1×1 mm^3 (http://www.bic.mni.mcgill.ca/ServicesAtlases/ICBM152NLin2009) [14]. This template was generated as an unbiased non-linear average among normal population in a broad range of age (18.5 to 43.5 years). The anatomical structures were segmented using ANIMAL+INSECT algorithm [15]. The cortical surface of the brain was extracted using SPM toolbox [16].

In general, there are multiple ways to estimate the locations of fNIRS measurements on the standard brain template. In the previous study [13], we have used a probabilistic registration procedure: Once the fNIRS probe was placed on a subject's head, the positions of optodes and five cranial landmarks (the nasion, the inion, the left and right preauricular points, and the vertex) were measured with a 3D digitizer (PatriotTM, Polhemus, Colchester, Vermont, U.S.A.). The cranial landmarks served as mediators for converting the real-world stereotaxic coordinates to the standard Montreal Neurological Institute (MNI) coordinates used in the brain template based on affine transformation [17].

2.2 Topography

The topography method in EasyTopo is derived based on the fact that the cortical layer of the brain is approximately a hemispherical surface. Thus, the stereotaxic coordinates of the brain surface in (x, y, z) is converted into the spherical coordinates in (r, θ, φ), in which the brain activation represents a distribution mainly in 2D (θ, φ) space. Then 2D angular interpolation is conducted in the (θ, φ) space to form a topographic image of the brain activation. Finally, by referring to the radius r, the topographic image in the (θ, φ) space is projected back onto the brain surface in the original 3D stereotaxic coordinates.

The original version of EasyTopo used a global stereotaxic coordinate system as well as a global spherical coordinate system which are defined in Figure 1(a). The θ-φ lattices (i.e., the latitude-longitude lattices), on which the channel-wise data are interpolated, are shown in Figures 1(b) and 1(c). One drawback of a global spherical coordinate system is that in the polar regions, which correspond to the temporal lobes of the brain, the θ-φ lattices are severely non-uniform as all of the longitude lines cross over. Therefore the interpolated image in the polar regions can be poor or completely wrong.

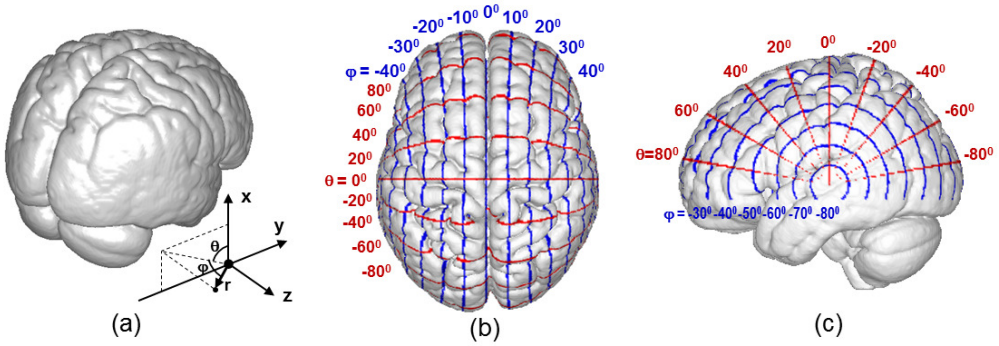

Figure 1. Default coordinate systems in the original version of EasyTopo: The global stereotaxic coordinates and the global spherical coordinates in (a) are used for data interpolation over the whole brain. The θ-φ lattices on the brain in the global spherical coordinate system are shown in (b) and (c).

To solve this problem, the latest version of EasyTopo implements the angular interpolation in two hemispheres separately. As shown in Figures 2(a) and 2(b), the *x*-*z* plane is rotated 50 degrees in each hemisphere, which generates more uniform θ-φ lattices on each hemisphere that are shown in Figures 2(c) and 2(d). Two topographic images are generated in two hemispheres separately and then combined together to form the activation map of the whole brain.

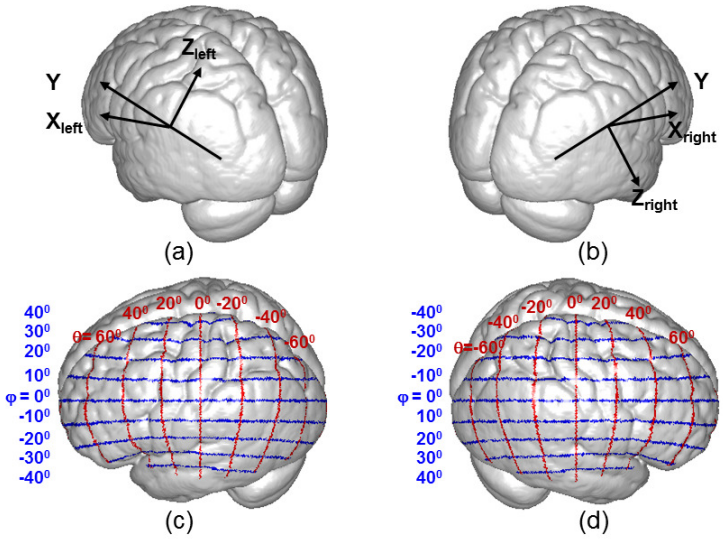

Figure 2. Default coordinate systems in the latest version of EasyTopo: The stereotaxic coordinates in (a) are for the left hemisphere and (b) are for the right hemisphere. In each hemisphere, the *x*-*z* plane is rotated 50 degree in order to generate more uniform θ-φ lattices, as shown in (c) and (d).

It is noted that EasyTopo does not require a globally constant radius (or a perfect spherical shape of the whole brain). It is because the data is interpolated only between the adjacent fNIRS measurements. As long as the radius is consistent in a sub-region defined by the adjacent measurements, the angular interpolation will be accurate. Figure 3(c) shows the distribution of radius of the brain surface in the spherical coordinate system given by Figures 3(a) and 3(b). Several representative cortical regions, such as the frontal, sensorimotor and visual cortices, do show a relatively consistent radius in Figure 3(c).

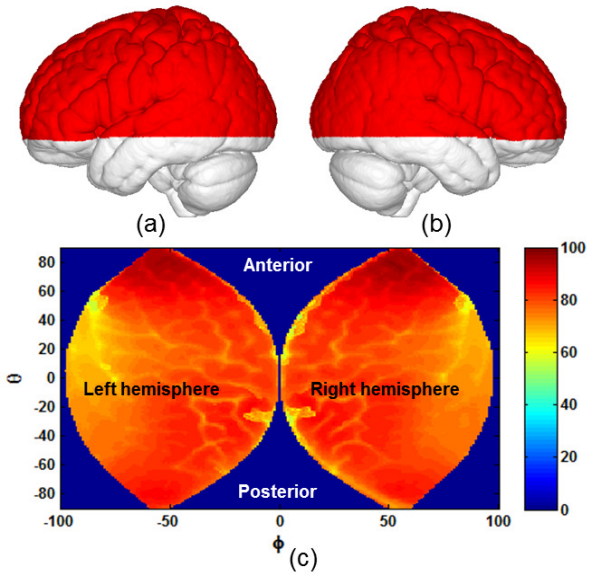

Figure 3. Default field of view (red) in EasyTopo on (a) the left hemisphere and (b) the right hemisphere, which covers the majority of the cortical areas that can be measured by fNIRS. After converting to the spherical coordinate systems, we can

represent the distribution of radius (in millimeter) of the brain surface in the (θ, φ) space for these two separate regions, as shown in (c).

Compared with the previous brain template-based topography methods [11,12], EasyTopo is more computationally efficient by using the 2D angular interpolation and does not require any data extrapolation. Another advantage of EasyTopo is that any data point between two adjacent measurements is interpolated along their included angle in the spherical coordinate system, rather than along a straight line going under the brain surface (see Figure 4(a)). The former interpolation is more physiologically meaningful and agrees better with the reality.

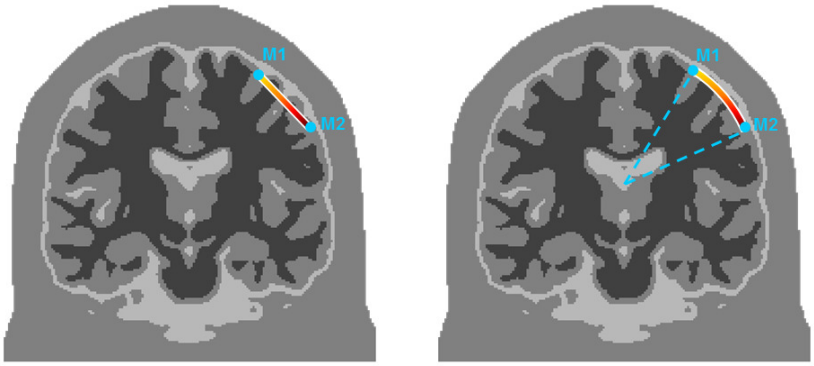

Figure 4. Schematic illumination of the difference between (a) the linear interpolation and (b) the angular interpolation. In linear interpolation, the data between two adjacent measurements, M1 and M2, is interpolated along a straight line that is actually under the surface of the brain. In angular interpolation, the data between M1 and M2 is interpolated along their included angle that agrees better with the surface of the brain.

2.3 Quantification

EasyTopo enables precise quantification of the size and location of the brain activation in the spherical coordination system. In general, the regions of interest (ROIs) can be determined by applying certain thresholds (e.g., the half maximum or half minimum) on the interpolated images in the (θ, φ) space. An example is shown in Figure 5. Once the ROIs are identified, the solid angle of each pixel in the identified ROIs is computed as:

$$\Omega_i = \cos\varphi_i d\varphi d\theta \tag{1}$$

where Ω_i and φ_i denote the solid angle and the polar angle of the ith pixel in the identified ROIs, respectively; $d\varphi$ and $d\theta$ denote the step of the polar angle and the step of the azimuthal angle, respectively.

Then the area of each identified ROI, A_{ROI}, can be estimated as:

$$A_{ROI} = \sum_{i \in ROI} \Omega_i r_i^2 \tag{2}$$

where r_i denotes the radius of the ith pixel in the identified ROIs.

The centroid of each identified ROI, (θ_c, φ_c), can be estimated as:

$$\theta_c = \frac{\sum_{i \in ROI} \theta_i \Omega_i r_i^2}{A_{ROI}} \tag{3}$$

and

$$\varphi_c = \frac{\sum_{i \in ROI} \varphi_i \Omega_i r_i^2}{A_{ROI}} \tag{4}$$

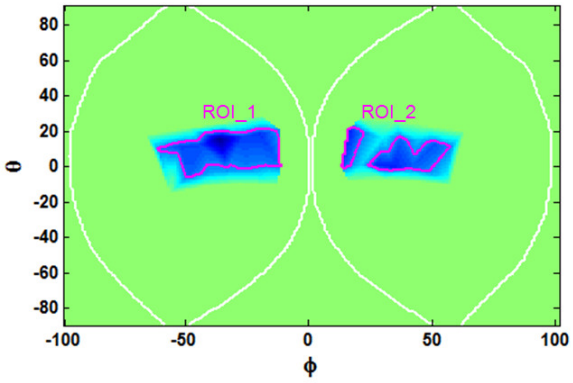

Figure 5. Example of identifying the ROIs of brain response in the (θ, φ) space: The bilateral brain response (in HbO_2 concentration) is evoked by 1-Hz repetitive transcranial magnetic stimulation (rTMS) over the left motor cortex [13]. The ROIs are identified as the regions below the half minimum of the image.

2.4 Validation

EasyTopo has been validated through both simulation and human experiments. In each case, the results of EasyTopo were compared with those from the rigorous depth-compensated diffuse optical tomography (DC-DOT) [18]. The geometry of the sparse optode array used in validation is shown in Figure 6(a), for both simulation and human measurements. The probe consisted of 6 light sources and 6 detectors, providing 15 measurements at an identical source-detector separation of 3.6 cm. The probe was placed over the primary sensorimotor cortex on the left hemisphere, as shown in Figure 6(b). In human experiment, the actual locations of the sources and detectors on the standard head template were determined through the probabilistic registration, as described in Section 2.1.

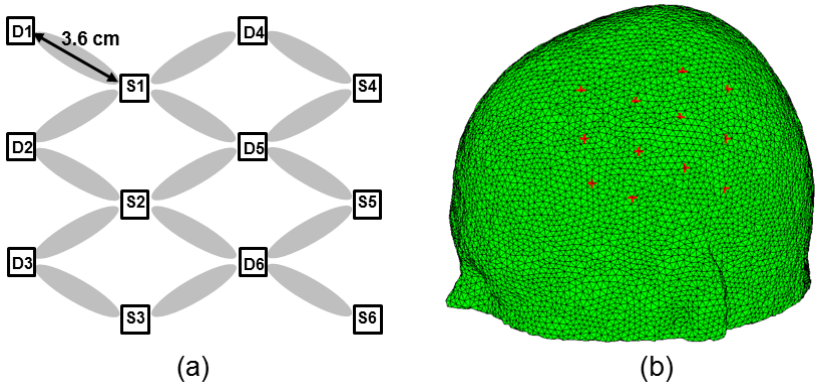

Figure 6. Probe and its cranial location in the simulation and human experiments: (a) The probe geometry. The probe consisted of 6 light sources and 6 detectors, providing 15 measurements at an identical source-detector separation of 3.6 cm. (b) The co-registered cranial location of the probe on the standard head template.

Simulation: A spherical absorber, 1.0 cm in diameter, was embedded just under the sensorimotor cortex to mimic a localized absorption change from the baseline caused by sensorimotor activation. The center of the absorber was about 2.2 cm in depth from the head surface. The background medium had an absorption coefficient of $\mu_a = 0.15$ cm^{-1} and a reduced scattering coefficient of $\mu_s' = 9.0$ cm^{-1} at 850 nm. The absorber had the same reduced scattering coefficient as the background, but a higher absorption coefficient of $\mu_a = 0.25$ cm^{-1} at 850 nm. Therefore, the absorber induced an absorption perturbation of $\Delta\mu_a = 0.10$ cm^{-1} to the background.

Human experiment: The human experiment used a common blocked-design paradigm which composed of 12 repetitive blocks, with 10 seconds of right-hand finger tapping and 20 seconds of rest per block [18]. A high-density DOT system (Cephalogics LLC., Boston, MA) was used to acquire data at 750 nm and 850 nm, using the probe geometry shown in Figure 6(a). The sampling rate was 10.8 Hz. The experiment protocol was approved by the University of Texas at Arlington Institutional Review Board. Written informed consent was obtained from every subject prior to the experiment.

Before either topographic or tomographic imaging, the human data was preprocessed through the following procedures: The channel-wise raw data in terms of light intensity were low-pass filtered at a cut-off frequency of 0.4 Hz to reduce the electronic noise and the fast-oscillating cardiac waves. Then the signal change in terms of optical density, ΔOD, was calculated. The calculated optical density changes were high-pass filtered at a cut-off frequency of 0.01 Hz to remove the long-term baseline drift during the experiment. Finally, for topography, the channel-wise hemoglobin changes were calculated based on the modified Beer-Lambert Law [19]; for tomography, the volumetric images in terms of optical density were reconstructed at each wavelength and then the hemoglobin images were calculated based on the Beer-Lambert Law [18].

For both simulation and human experiments, the topographic and tomographic images of the sensorimotor activation were generated and analyzed through the following procedures:

Topography: The location of each measurement was determined as the midpoint between its corresponding light source and detector. As shown in Figure 7(a), the 15 measurement points defined a dashed rectangle region that was smaller than the actual coverage of the probe. To solve this problem, we added a virtual boundary to enlarge the region of topography: the virtual boundary was defined by the boundary optodes, which is the solid rectangle region shown in Figure 7(a). The corresponding values at the boundary optodes were forced to be zero since little light propagated beyond the boundary optodes. Figures 7(b) and 7(c) compare the interpolated images without and with adding the virtual boundary. Apparently the image generated with the virtual boundary is better.

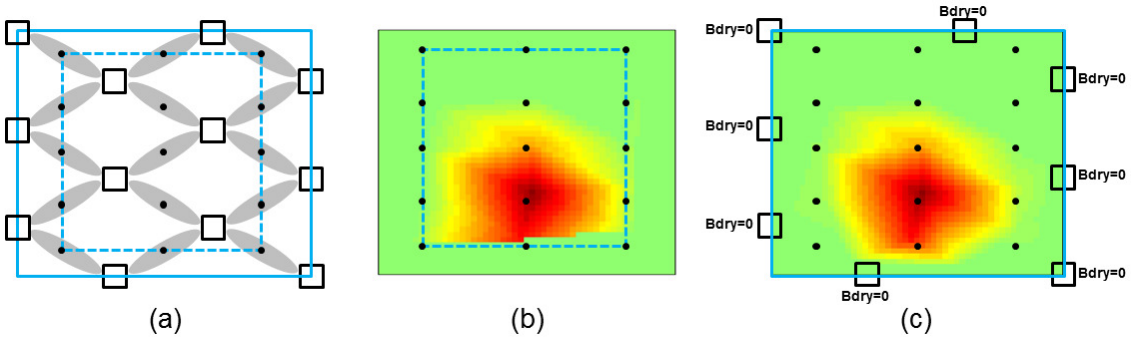

Figure 7. Comparison of diffuse optical topography without and with adding the virtual boundary: (a) The regions of topography without (dashed rectangle) and with (solid rectangle) adding the virtual boundary. The small squares represent the optodes and the solid dots represent the midpoints of measurements. Without adding the virtual boundary, the region of topography defined by the 15 measurement points is smaller than the actual coverage of the probe. (b) The interpolated image without adding the virtual boundary. The image is generated in the smaller region (dashed rectangle) defined by the 15 measurement points (solid dots). (c) The interpolated image after adding the virtual boundary with forced zeros at the boundary optodes.

Tomography: The details of DC-DOT have been described in our recent report [18]. DC-DOT can localize the brain activation very closely to its actual depth. An example is shown in Figure 8(a). To compare the images generated by EasyTopo and DC-DOT, we selected an 'arc' region on the brain surface (1.5 to 2.5 cm in depth) as indicated in Figure 8(a). The tomographic image within this region was averaged across depth to generate a surface image of the brain activation. Such a surface image was in the same format as a topographic image so that they could be compared directly.

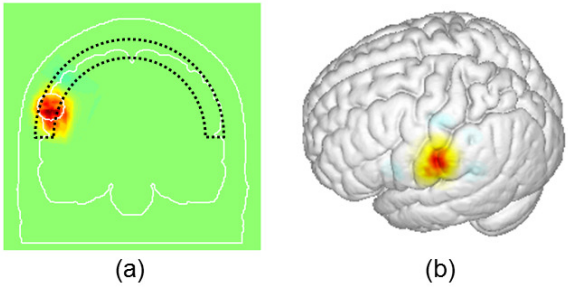

Figure 8. Visualization of a volumetric image generated by DC-DOT: (a) A coronal view of the brain activation induced by a finger tapping task. By using the depth compensation algorithm [18], the activation is recovered right on the cortical

surface of the brain. An 'arc' region on the surface of the brain is selected for further visualization of the brain activation. (b) A surface image of the brain activation generated by averaging the hemodynamic changes within the 'arc' region across depth.

3. RESULTS

3.1 Results from simulation

Figure 9(a) shows the distribution of the actual absorption perturbation induced by the static absorber in the (θ, φ) space. Figure 9(b) shows the (θ, φ) map generated by EasyTopo, and Figure 9(c) shows the (θ, φ) map generated by DC-DOT, respectively. In both Figures 9(b) and 9(c), the recovered distributions of absorption perturbation are blurred and larger than the actual absorption distribution. The centroids of both images also slightly deviated from the actual position. Besides the blurring and the centroid shifting from the actual absorption perturbation, the topographic image generated by EasyTopo and the tomographic image generated by DC-DOT agree well with one another.

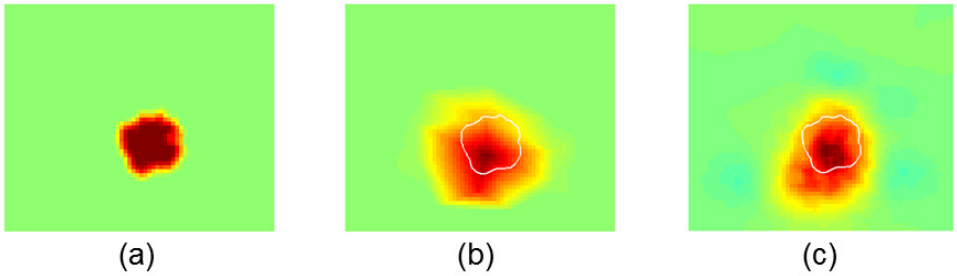

Figure 9. Comparison of (a) the actual absorption perturbation, (b) the recovered image by EasyTopo, and (c) the recovered image by DC-DOT in the (θ, φ) space in the simulation experiment. The white circles in (b) and (c) indicate the actual regions of the absorption perturbation.

Figures 10(a) to 10(c) show the actual absorption perturbation, the topographic image generated by EasyTopo, and the tomographic image generated by DC-DOT after we projected the actual and reconstructed absorption images onto the surface of the standard brain. The surface images derived from EasyTopo and DC-DOT are very similar to one another.

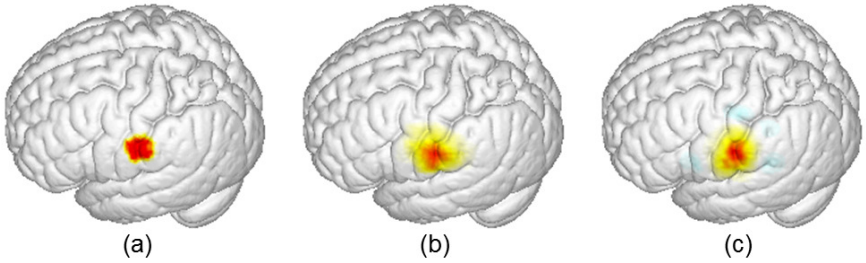

Figure 10. Brain surface images of (a) the actual absorption perturbation, (b) the recovered absorption perturbation by EasyTopo, and (c) the recovered absorption perturbation by DC-DOT in the simulation experiment.

3.2 Results from human finger tapping measurement

Figure 11 shows the block-averaged HbO_2 changes due to a finger tapping task [18] from all of the 15 channels (subject 1). A robust increase of HbO_2 concentration is seen during and shortly after the task. According to Figure 11, we averaged the data between 0 to 15 seconds to generate the topographic and tomographic images.

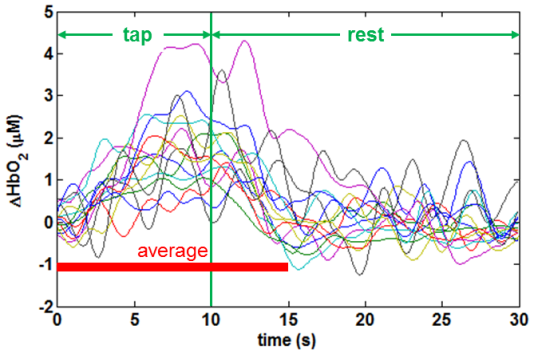

Figure 11. Block-averaged HbO_2 changes due to the finger tapping task from all of the 15 channels (subject 1). A robust increase of HbO_2 concentration is seen during and shortly after the finger tapping task.

Figures 12(a) and 12(b) show the (θ, φ) maps of the sensorimotor activation generated by EasyTopo and DC-DOT, respectively. The centroids of the sensorimotor activation are slightly different between two images. We expect the topographic image, i.e., Figure 12(a), has slightly bigger localization error. It is because in EasyTopo, the position of each measurement was determined as the midpoint between its corresponding light source and detector, which was arbitrary by considering the actual optical pathway through the complex brain structures. On the other hand, DC-DOT computes the light propagation through the brain rigorously. Therefore, it should provide us with a more accurate reconstructed image.

Figures 12(c) and 12(d) show the topographic and tomographic images of the sensorimotor activation after the reconstructed images are projected onto the surface of the standard brain, respectively. Both images demonstrate activation across the primary motor and primary sensory gyri during the finger tapping task.

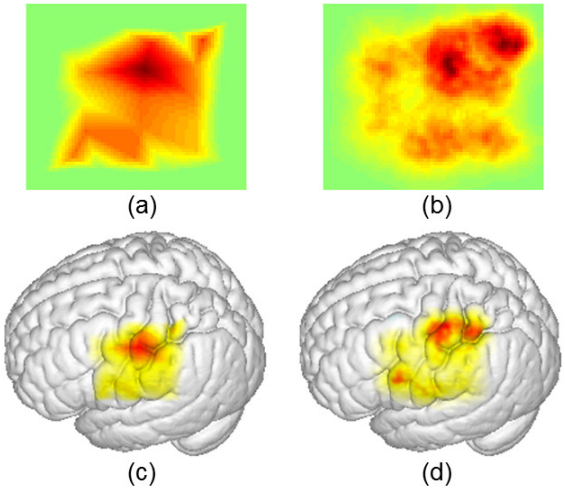

Figure 12. Recovered sensorimotor activations in human experiment: (a) the (θ, φ) map and (c) the brain surface image of the sensorimotor activation generated by EasyTopo; (b) the (θ, φ) map and (d) the brain surface image of the sensorimotor activation generated by DC-DOT. Both (c) and (d) demonstrate activation across the primary motor and primary sensory gyri during the finger tapping task.

4. DISCUSSION

We have developed the EasyTopo toolbox for rapid diffuse optical topography based on a standard brain template. Compared with the previous topography methods [11,12], EasyTopo is more computationally efficient by conducting 2D angular interpolation in a spherical coordinate system. Moreover, the angular interpolation is more physiologically meaningful and agrees better with the realistic brain structures. We also validated EasyTopo through both simulation and human experiments. For a sparse probe geometry, the performance of EasyTopo is close to that of a rigorous

tomography approach (DC-DOT), while the former one avoids solving the forward and inverse problems of light propagation.

Since the optical pathway through the brain is not computed, EasyTopo estimates the location of each measurement as the midpoint between its corresponding light source and detector. This approximation induces two problems: first, for some probe geometries, e.g., the one shown in Figure 7(a), the region defined by the measurement points is smaller than the actual coverage of the probe. To solve this problem, a virtual boundary defined by the boundary optodes can be added to enlarge the region of topography, as we demonstrated in Figure 7(c). Second, this approximation possibly induces a slight positional error into the image, as compared to DC-DOT, as indicated in Figures 12(a) and 12(b). However, given the sparsity of the measurements often made in most clinical applications, we believe such a positional error is negligible.

At last, it is noted that in principle diffuse optical topography should not be used in high-density fNIRS measurements. As we have demonstrated in a recent study [18], DC-DOT can generate much more accurate volumetric images to show brain activations when using high-density measurements.

5. ACKNOWLEDGEMENTS

The authors would like to thank Dr. Xu Cui at Department of Psychiatry and Behavioral Sciences, Stanford University, for the helpful discussion on the brain template-based topography. This work was supported in part by NIH Grant R01 (5R33CA101098).

REFERENCES

[1] Villringer, A., Planck, J., Hock, C., Schleinkofer, L. and Dirnagl, U., "Near infrared spectroscopy (NIRS): a new tool to study hemodynamic changes during activation of brain function in human adults," Neurosci. Lett. 154(1-2), 101-104 (1993).

[2] Hoshi, Y. and Tamura, M., "Detection of dynamic changes in cerebral oxygenation coupled to neuronal function during mental work in man," Neurosci. Lett. 150(1), 5-8 (1993).

[3] Chance, B., Zhuang, Z., UnAh C., Alter, C. and Lipton, L., "Cognition-activated low-frequency modulation of light absorption in human brain," Proc. Natl. Acad. Sci. USA 90, 2660-2774 (1993).

[4] Maki, A., Yamashita, Y., Ito, Y., Watanabe, E., Mayanagi, Y. and Koizumi, H. "Spatial and temporal analysis of human motor activity using noninvasive NIR topography," Med. Phys. 22(12), 1997-2005 (1995).

[5] Franceschini, M.A., Toronov, V., Filiaci, M., Gratton, E. and Fanini, S., "On-line optical imaging of the human brain with 160-ms temporal resolution," Optics Express 6, 49-57 (2000).

[6] Boas, D.A., Chen, K., Grebert, D. and Franceschini, M.A., "Improving the diffuse optical imaging spatial resolution of the cerebral hemodynamic response to brain activation in humans," Optics Letters 29, 1506-1509 (2004).

[7] Zeff, B.W., White, B.R., Dehghani, H., Schlaggar, B.L. and Culver, J.P., "Retinotopic mapping of adult human visual cortex with high-density diffuse optical tomography," Proc. Natl. Acad. Sci. USA. 104(29), 12169-12174 (2007).

[8] White, B.R. and Culver, J.P., "Quantitative evaluation of high-density diffuse optical tomography: in vivo resolution and mapping performance," J. Biomed. Opt. 15, 026006 (2010).

[9] Eggebrecht, A.T., White, B.R., Ferradal, S.L., Chen, C., Zhan, Y., Snyder, A.Z., Dehghani, H. and Culver J.P., "A quantitative spatial comparison of high-density diffuse optical tomography and fMRI cortical mapping," NeuroImage 61(4), 1120-1128 (2012).

[10] Zhan, Y., Eggebrecht, A.T., Culver, J.P. and Dehghani, H., "Image quality analysis of high-density diffuse optical tomography incorporating a subject-specific head model," Front Neuroenergetics 4, 6 (2012).

[11] Ye, J.C., Tak, S., Jang, K.E., Jung, J. and Jang, J., "NIRS-SPM: statistical parametric mapping for near-infrared spectroscopy," NeuroImage 44(2), 428-447 (2009).

[12] Cui, X., Bray, S., Bryant, D. M., Glover, G. H. and A. L. Reiss, "A quantitative comparison of NIRS and fMRI across multiple cognitive tasks," NeuroImage 54(4), 2808-2821 (2011).

[13] Tian, F., Kozel, A., Yennu, A., Croarkin, P.E., McClintock, S.M., Mapes, K.S., Husain, M.M. and Liu H., "Test-retest assessment of cortical activation induced by repetitive transcranial magnetic stimulation with brain atlas-guided optical topography," J. Biomed. Opt. 17(11), 116020 (2012).
[14] Fonov, V.S., Evans, A.C., McKinstry, R.C., Almli, C.R. and Collins D.L., "Unbiased nonlinear average age-appropriate brain templates from birth to adulthood," NeuroImage 47, S102-S102 (2009).
[15] Collins, D.L., Zijdenbos, A.P., Baaré, W.F.C. and Evans, A.C., "ANIMAL+INSECT: Improved Cortical Structure Segmentation," IPMI Lecture Notes in Computer Science 1613, 210-223 (1999).
[16] Friston, K., Ashburner, J. and Kiebel, S., [Statistical Parametric Mapping: The Analysis of Functional Brain Images, 1st Edition] Elsevier Science & Technology Books (2007).
[17] Singh, A.K., Okamoto, M., Dan, H., Jurcak, V. and Dan, I., "Spatial registration of multichannel multi-subject fNIRS data to MNI space without MRI," NeuroImage 27(4), 842-851 (2005).
[18] Tian F. and Liu H., "Depth-compensated diffuse optical tomography (DC-DOT) of sensorimotor activation based on a standard template of brain atlas," NeuroImage (2013) (under peer review).
[19] Cope., M., Delpy., D. T., Reynolds, E. O., Wray, S., Wyatt, J. and van der Zee P., "Methods of quantitating cerebral near infrared spectroscopy data," Adv. Exp. Med. Biol. 222, 183-189 (1988).